Title

Carbon isotopes characterize rapid changes in atmospheric carbon dioxide during the last deglaciation

Journal

Proceedings of the National Academy of Sciences of the United States of America, 113(13)

ISSN

0027-8424

Authors

Bauska, Thomas K
Baggenstos, Daniel
Brook, Edward J
et al.

Publication Date

2016-03-29

DOI

10.1073/pnas.1513868113

Peer reviewed

Carbon isotopes characterize rapid changes in atmospheric carbon dioxide during the last deglaciation

Thomas K. Bauska[a,b,1], Daniel Baggenstos[c], Edward J. Brook[a], Alan C. Mix[a], Shaun A. Marcott[d], Vasilii V. Petrenko[e], Hinrich Schaefer[f], Jeffrey P. Severinghaus[c], and James E. Lee[a]

[a]College of Earth, Ocean, and Atmospheric Sciences, Oregon State University, Corvallis, OR 97331; [b]Department of Earth Sciences, University of Cambridge, Cambridge CB2 3EQ, United Kingdom; [c]Scripps Institution of Oceanography, University of California, San Diego, La Jolla, CA 92093; [d]Department of Geoscience, University of Wisconsin—Madison, Madison, WI 53706; [e]Department of Earth and Environmental Sciences, University of Rochester, Rochester, NY 14627; and [f]Climate and Atmosphere Center, National Institute of Water and Atmospheric Research Ltd, Wellington, New Zealand 6023

Edited by Mark H. Thiemens, University of California, San Diego, La Jolla, CA, and approved February 2, 2016 (received for review July 17, 2015)

An understanding of the mechanisms that control CO_2 change during glacial–interglacial cycles remains elusive. Here we help to constrain changing sources with a high-precision, high-resolution deglacial record of the stable isotopic composition of carbon in CO_2 ($\delta^{13}C$-CO_2) in air extracted from ice samples from Taylor Glacier, Antarctica. During the initial rise in atmospheric CO_2 from 17.6 to 15.5 ka, these data demarcate a decrease in $\delta^{13}C$-CO_2, likely due to a weakened oceanic biological pump. From 15.5 to 11.5 ka, the continued atmospheric CO_2 rise of 40 ppm is associated with small changes in $\delta^{13}C$-CO_2, consistent with a nearly equal contribution from a further weakening of the biological pump and rising ocean temperature. These two trends, related to marine sources, are punctuated at 16.3 and 12.9 ka with abrupt, century-scale perturbations in $\delta^{13}C$-CO_2 that suggest rapid oxidation of organic land carbon or enhanced air–sea gas exchange in the Southern Ocean. Additional century-scale increases in atmospheric CO_2 coincident with increases in atmospheric CH_4 and Northern Hemisphere temperature at the onset of the Bølling (14.6–14.3 ka) and Holocene (11.6–11.4 ka) intervals are associated with small changes in $\delta^{13}C$-CO_2, suggesting a combination of sources that included rising surface ocean temperature.

ice cores | paleoclimate | carbon cycle | atmospheric CO_2 | last deglaciation

Over thirty years ago ice cores provided the first clear evidence that atmospheric CO_2 increased by about 75 ppm as Earth transitioned from a glacial to an interglacial state (1, 2). After decades of research, the underlying mechanisms that drive glacial–interglacial CO_2 cycles are still unclear. A tentative consensus has formed that the deglaciation is characterized by a net transfer of carbon from the ocean to the atmosphere and terrestrial biosphere, through a combination of changes in ocean temperature, nutrient utilization, circulation, and alkalinity. Partitioning these changes in terms of magnitude and timing is challenging. Estimates of the glacial–interglacial carbon cycle budget are highly uncertain, ranging from 20–30 ppm for the effect of rising ocean temperature, 5–55 ppm for ocean circulation changes, and 5–30 ppm for decreasing iron fertilization (3, 4), with feedbacks from $CaCO_3$ compensation accounting for up to 30 ppm (5, 6).

A precise history of the stable isotopic composition of atmospheric carbon dioxide ($\delta^{13}C$-CO_2) can constrain key processes controlling atmospheric CO_2 (7, 8). A low-resolution record from the Taylor Dome ice core (9) identified a decrease in $\delta^{13}C$-CO_2 at the onset of the deglacial CO_2 rise that was followed by increases in both CO_2 and $\delta^{13}C$-CO_2 (Fig. 1). A higher-resolution record from the European Project for Ice Coring in Antarctica Dome C (EDC) ice core (10) provided additional support for the rapid $\delta^{13}C$-CO_2 decrease associated with the initial CO_2 rise, and box modeling indicated that this decrease was consistent with changes in marine productivity. The record also included other rapid changes in $\delta^{13}C$-CO_2, albeit at low precision, supporting large variations of organic carbon fluxes, notably a sharp increase in $\delta^{13}C$-CO_2 during the Bølling–Allerød (BA) interval attributed to carbon uptake by the terrestrial biosphere. A combined record including higher-precision EDC and Talos Dome data (11) documented a $\delta^{13}C$-CO_2 decrease beginning near 17.5 ka. This shift in $\delta^{13}C$-CO_2 was interpreted to indicate that some process in the Southern Ocean (SO), possibly changes in upwelling, drove the initial CO_2 rise. This previous work did not resolve high-frequency variability in the $\delta^{13}C$-CO_2 records that may be essential for discerning mechanisms of change.

Here we use an analytical method (12) that employs dual-inlet isotope ratio mass-spectrometry to obtain precision approaching that of modern atmospheric measurements [~0.02‰ 1-sigma pooled SD based on replicate analysis compared with ~0.05–0.11‰ for previous studies (9–11)]. We extracted atmospheric gases from large (400–500 g) samples taken from surface outcrops of ancient ice at Taylor Glacier, Antarctica, at an average temporal resolution of 165 y between 20 and 10 ka, and subcentury resolution during rapid change events. This resolution allows us to delineate isotopic fingerprints of rapid shifts in CO_2 that were previously impossible to resolve. Our study complements recent precise observations of CO_2 concentration variations during the last deglaciation, which revealed abrupt centennial-scale changes (13) (Fig. 2).

During the initial 35-ppm CO_2 rise from 17.6 to 15.5 ka, we find a 0.3‰ decrease in $\delta^{13}C$-CO_2 that is interrupted by a sharp minimum coincident with rapid increases in CO_2 and CH_4 around 16.3 ka (13, 14) (Fig. 2). The 16.3-ka feature in the CO_2 and CH_4 concentration records, which corresponds to a 0.1‰ negative excursion in $\delta^{13}C$-CO_2, has been plausibly tied to the timing of Heinrich event 1 (13, 14) and signals a mode switch in the deglacial

Significance

Antarctic ice cores provide a precise, well-dated history of increasing atmospheric CO_2 during the last glacial to interglacial transition. However, the mechanisms that drive the increase remain unclear. Here we reconstruct a key indicator of the sources of atmospheric CO_2 by measuring the stable isotopic composition of CO_2 in samples spanning the period from 22,000 to 11,000 years ago from Taylor Glacier, Antarctica. Improvements in precision and resolution allow us to fingerprint CO_2 sources on the centennial scale. The data reveal two intervals of rapid CO_2 rise that are plausibly driven by sources from land carbon (at 16.3 and 12.9 ka) and two others that appear fundamentally different and likely reflect a combination of sources (at 14.6 and 11.5 ka).

Author contributions: T.K.B., D.B., E.J.B., A.C.M., V.V.P., and J.P.S. designed research; T.K.B., D.B., S.A.M., V.V.P., H.S., and J.E.L. performed research; T.K.B. and D.B. analyzed data; and T.K.B. wrote the paper with input from all authors.

The authors declare no conflict of interest.

This article is a PNAS Direct Submission.

Data deposition: Date are deposited at the National Climatic Data Center (NOAA), https://www.ncdc.noaa.gov/paleo/study/19765

[1]To whom correspondence should be addressed. Email: tkb28@cam.ac.uk.

This article contains supporting information online at www.pnas.org/lookup/suppl/doi:10.1073/pnas.1513868113/-/DCSupplemental.

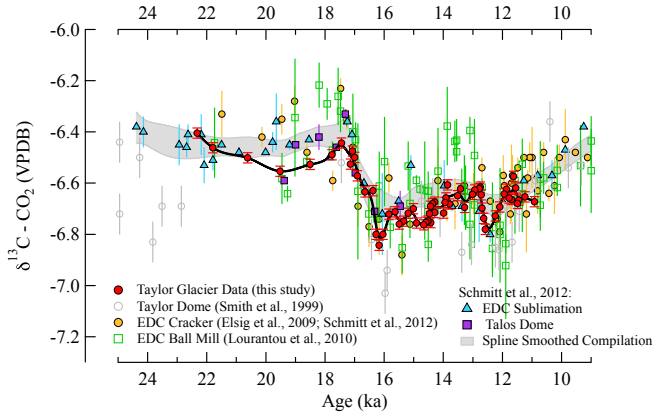

Fig. 1. Carbon isotope records during the last deglaciation. Taylor Glacier δ^{13}C-CO_2 data from this study (red). Previous work from Taylor Dome (gray open circles) (9), Grenoble EDC data (open green squares) (10), Bern EDC data (orange circles) (11, 45), sublimation measurements from EDC (blue triangles), and Talos Dome (purple squares) with an estimate of the 1-sigma uncertainty from a compilation of previous ice core δ^{13}C-CO_2 data (11).

CO_2 rise. The subsequent slower rise in CO_2 from 15.5 to 14.8 ka is not accompanied by large changes in δ^{13}C-CO_2. Across the Oldest Dryas to Bølling transition (14.6–14.3 ka) and coincident with a 10-ppm CO_2 increase and large CH_4 increase, we resolve a 0.08‰ increase in δ^{13}C-CO_2 (Fig. 2). Rapid increases in CO_2 and CH_4 at the Younger Dryas (YD) to Preboreal transition (11.6–11.4 ka) are associated with minor variability δ^{13}C-CO_2. On the other hand, the onset of the YD (12.8–12.5 ka) is characterized by a small rise in CO_2 associated with a 0.15‰ decrease in δ^{13}C-CO_2 that appears tightly coupled to the timing of the large CH_4 decrease. The recovery from this excursion is characterized by increasing CO_2 and δ^{13}C-CO_2. Broadly, our data confirm the results of Schmitt et al. (11) (Fig. 1). However, some of the large swings in δ^{13}C-CO_2 indicated by the earlier EDC record (10), may be inaccurate and require reexamination.

Processes Controlling Atmospheric δ^{13}C-CO_2

To visualize the constraints provided by δ^{13}C-CO_2 on the processes controlling CO_2 we use a cross-plot of CO_2 and δ^{13}C-CO_2 (referred to as a Keeling plot when the x axis is equal to $1/CO_2$). When the classic Keeling plot is applied to a two-component system, and assuming conservation of mass, the y axis intercept of a linear regression to the data (y_0) approximates the δ^{13}C signature of a secondary external source mixing with a primary source (15). In the more complex mixing between the atmosphere, ocean, and terrestrial biosphere, y_0 is still indicative of the source reservoir's δ^{13}C signature but interpretation requires a model of the carbon cycle to account for processes such as air–sea gas exchange, ocean mixing, and ocean–sediment interactions, which buffer the atmospheric δ^{13}C-CO_2 signature over long timescales and reduce the slope of δ^{13}C:1/[CO_2] (7). We use a simple box model of the carbon cycle, previously published box model experiments (7) and intermediate complexity models to account for these effects and deconvolve the processes responsible for the deglacial rise in CO_2. We divide the processes into the following categories: ocean productivity and circulation, land carbon storage (particularly rapid changes), ocean temperature, the $CaCO_3$ cycle, and air–sea gas exchange. Individual model Keeling plot intercepts are listed in *SI Appendix*, Table S1; the ranges within each category are represented graphically in Fig. 3*A*.

An oceanic δ^{13}C-DIC depth gradient is controlled by a combination of ocean mixing and export from the surface of isotopically light organic carbon. Decreased carbon export or increased ocean ventilation during the last deglaciation would decrease the δ^{13}C-DIC gradient, leading to a rise in atmospheric CO_2 and decrease in atmospheric δ^{13}C-CO_2. First, we simulate a plausible signature of a glacial–interglacial weakening of the marine biological pump by forcing a decrease in the strength of the Subantarctic biological pump from near full efficiency (PO_4 = 0.2 mmol m^{-3}) to preindustrial level (PO_4 = 1.4 mmol m^{-3}). The timing of this change is scaled to the decrease in dust delivery to Antarctica (16). This leads to an increase in CO_2 and decrease of δ^{13}C-CO_2; the relationship is characterized in our model with y_0 equal to −8.6‰. For comparison, factorial experiments with the Bern 3D model of the last glacial–interglacial cycle isolate the effect of iron fertilization in the model (17) with a resultant Keeling intercept of −9.6‰. Second, we vary the rate of SO upwelling in our box model. Greater ocean ventilation raises CO_2 and lowers δ^{13}C-CO_2 resulting in a Keeling plot intercept of −8.4‰. Experiments with the Bern 3D model where wind stress over the SO was varied (20–180%) show that atmospheric CO_2 positively correlates with the rate of ocean overturning (18). The simulated CO_2 and δ^{13}C-CO_2 produce a Keeling plot intercept between −7.6‰ [when the Atlantic Meridional Overturning Circulation (AMOC) is in an "on" state] and −8.6‰ (when AMOC is in an "off" state). Finally, decreased AMOC has been hypothesized to slow the delivery of low preformed nutrient water to the deep ocean and consequently drive a weakening of the biological pump. Experiments with the Model of Ocean Biogeochemistry and Isotopes/University of Victoria climate model of intermediate

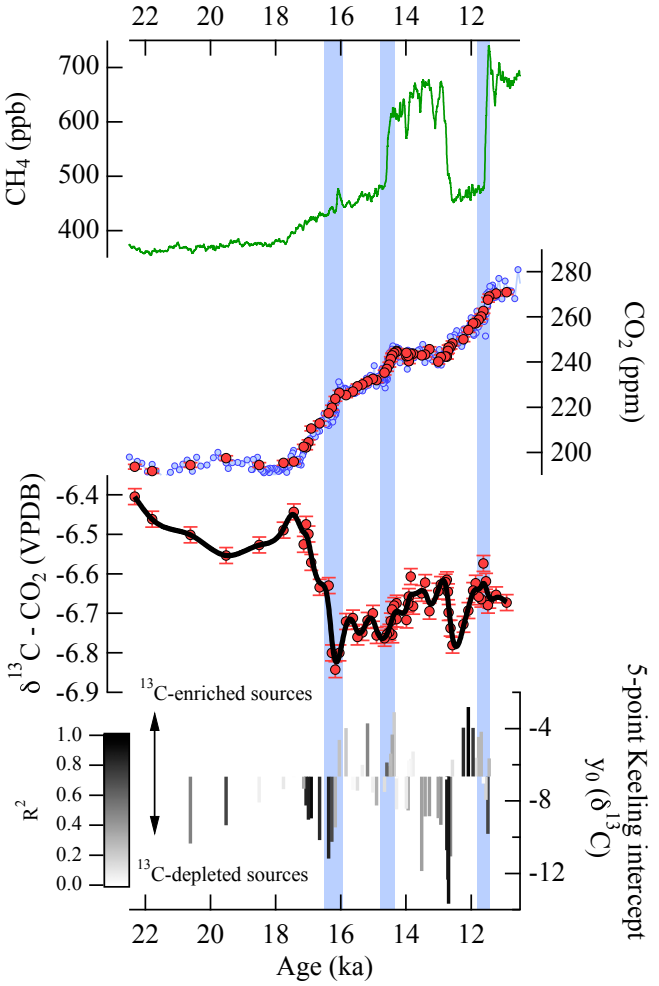

Fig. 2. Carbon cycle changes of the last deglaciation. WAIS Divide continuous CH_4 (green) (14) and discrete CO_2 (blue) (13) concentration data plotted with Taylor Glacier CO_2 and δ^{13}C-CO_2 data (this study) (red markers, black line is a smoothing spline), the five-point running Keeling intercept with shading indicating the R^2 for each time interval. Blue bars indicate intervals of rapid CO_2 rise identified in the WAIS Divide ice core (13).

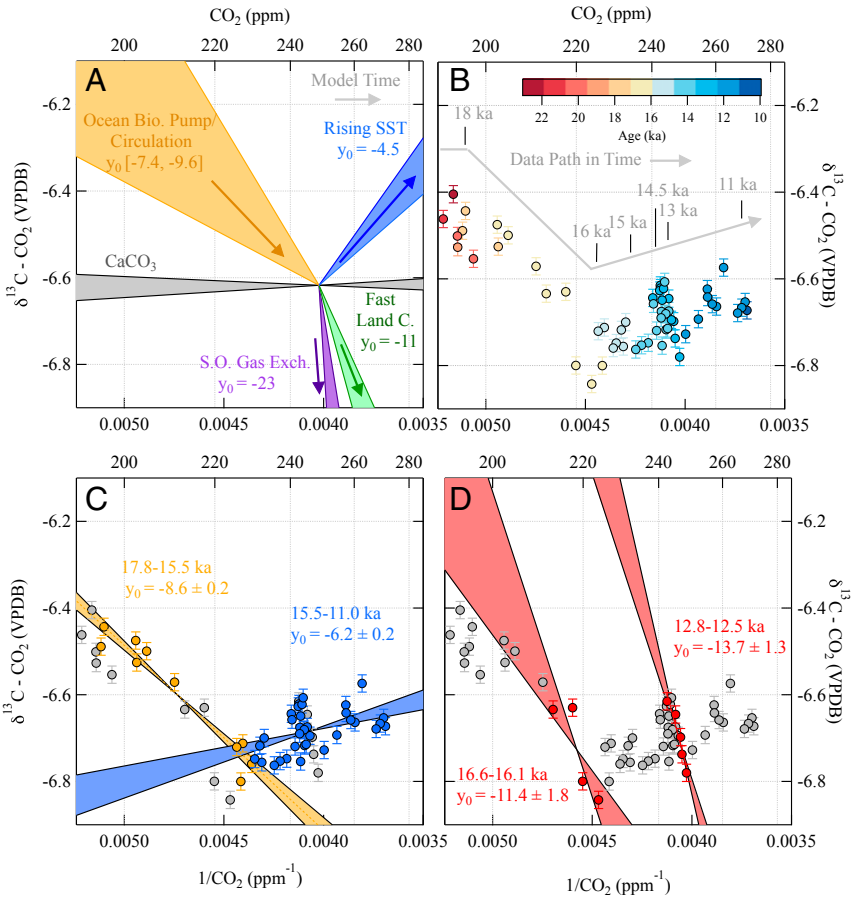

Fig. 3. Cross-plot of data constraints and model experiments. (*A*) Shaded lines show the range of model-based constraints on various carbon cycle processes as listed in *SI Appendix*, Table S1 (changes in ocean biological pump/circulation, yellow; deglacial increase in SST, blue; rapid release of land carbon, green; rapid change in Southern Ocean gas exchange, purple; $CaCO_3$ cycle, gray). (*B*) All Taylor Glacier data with arrows as guides to the approximate time path. (*C*) The data divided into the early HS1 (yellow) and later deglaciation (blue) modes of variability. Colored markers divide the data by time period and the shaded vectors indicate the linear regressions of the data with the 1-sigma uncertainty. (*D*) Further division of the data into the abrupt changes at The 16.3-ka event and onset of the YD (red). See *SI Appendix*, Table S2 for statistics.

complexity that simulated an interval of collapsed AMOC show atmospheric CO_2 rising and $\delta^{13}C$-CO_2 decreasing (19) (y_0 = −8.5‰). Combining all these experiments provides plausible constraints on oceanic sources to the atmosphere (y_0 ~= −7.4 to −9.6‰), which include both productivity driven changes (e.g., iron fertilization) and deep-ocean ventilation change (e.g., enhanced turnover of deep water masses) (Fig. 3*A*).

During the deglaciation, the release of oceanic carbon to the atmosphere is likely partially offset by the gradual accumulation of carbon on land, primarily during the later part of the deglaciation when the major ice sheets are small and dwindling (14–10 ka) (20). This land carbon uptake would lower atmospheric CO_2 and increase $\delta^{13}C$-CO_2. Because the magnitude of carbon isotopic fractionation by photosynthesis is very similar in the marine and terrestrial regimes, changes in organic carbon cycling between the land, atmosphere, and ocean that are slower than the timescale of ocean mixing are broadly indistinguishable from the atmospheric data alone. However, for changes in organic land carbon storage that are rapid relative to the mixing time of carbon in the ocean–atmosphere system, the atmospheric signal will more closely reflect the isotopic signature of organic carbon and then diminish as it is buffered by exchange with the deep ocean. We drive changes in atmospheric CO_2 of about 10 ppm by varying the land-to-atmosphere carbon flux in our model at periodicities of 50, 500, and 5,000 y. The change in $\delta^{13}C$-CO_2 decreases with increasing periodicity resulting in y_0 of −13.4‰, −10.9‰, and −9.8‰ at the 50, 500, and 5,000 y periodicities, respectively. Fast land carbon fluxes to the atmosphere can therefore be distinguished from changes in the ocean biological pump with high-resolution atmospheric data (y_0 = ~<−10.9‰; Fig. 3*A*).

Increasing ocean temperature decreases both the solubility of CO_2 in seawater and the magnitude of isotopic fractionation during air–sea gas exchange. Rising atmospheric CO_2 and increasing $\delta^{13}C$-CO_2 are therefore consistent with ocean warming. Forcing our model with latitudinal temperature stacks (21) for the deglaciation results in a 35-ppm rise in atmospheric CO_2 with an increase of about 0.3‰ in $\delta^{13}C$-CO_2 with an apparent y_0 from this effect of −4.5‰ (Fig. 3*A*).

Carbon isotopic fractionation during $CaCO_3$ formation from seawater is very small compared with that of photosynthesis, and the $\delta^{13}C$ of CO_2 from volcanic emissions, though poorly constrained, is very similar to atmospheric values. Processes like $CaCO_3$ compensation, reef building, and volcanic emissions are thus consistent with rising CO_2 and little to no change in $\delta^{13}C$-CO_2 (y_0 = initial atmospheric $\delta^{13}C$-CO_2; Fig. 3*A*). Moreover, a decrease in the amount of respired carbon in the deep ocean, driven by either oceanic changes or land carbon regrowth, will trigger increases in $CaCO_3$ preservation (and corresponding production of CO_2) that act to restore $[CO_3^{2-}]$ over multimillennial timescales (22, 23). The indirect effect of a weakened biological pump or land carbon regrowth would thus be an increase in CO_2 with little change in $\delta^{13}C$-CO_2 over thousands to tens of thousands of years. In Keeling plot space the inferred intercept of a weakened biological pump would slowly asymptote to the $CaCO_3$ intercept. On even longer timescales the $\delta^{13}C$-CO_2 signature of all processes is dampened toward a steady state determined by the input of volcanic and weathering fluxes of carbon to the atmosphere/ocean (10^5 y) (24). The box model experiments presented here largely exclude $CaCO_3$ feedbacks (*SI Appendix*) and thus represent only the direct effect of various carbon cycle processes that are important in constraining the isotope signature on the centennial-to-millennial timescale, at the expense of underestimating the long-term feedbacks that are significant on glacial–interglacial timescales.

Changes in air–sea gas exchange, via changes in sea-ice extent or wind speed in the SO, are hypothesized to have a significant impact on CO_2 and $\delta^{13}C$-CO_2, generally with increased air–sea

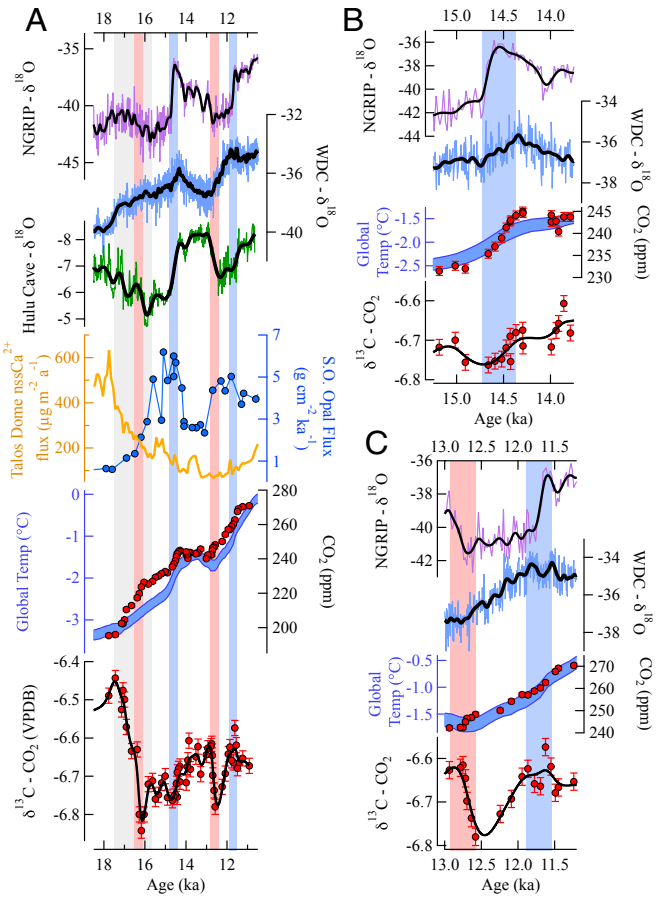

Fig. 4. Climate and carbon cycle changes during the last deglaciation. (*A*) Proxies for Greenland temperature (46) (purple), West Antarctic temperature (37, 47) (blue), East Asian precipitation (48) (green), dust delivery to Antarctica (30) (yellow), Southern Ocean upwelling (31) (blue markers), global temperature relative to the early Holocene (blue banding) (21), and the Taylor Glacier CO_2 and $\delta^{13}C$-CO_2 data (red). The red bars indicate periods of rapid $\delta^{13}C$-CO_2 decreases; blue bars indicate rapid CO_2 increases with slight increases or little change in $\delta^{13}C$-CO_2. *B* and *C* highlight the changes in temperature and atmospheric CO_2 at the centennial scale.

gas exchange leading to increases in atmospheric CO_2 and large decreases in $\delta^{13}C$-CO_2 (7, 25). In our model, varying the air–sea gas exchange coefficient over the SO by ±50% over periods of 50, 500, and 5,000 y (but keeping ocean mixing constant) produces small rises in CO_2 and a sharp decrease in $\delta^{13}C$-CO_2 when air–sea gas exchange is enhanced. Keeling plot intercepts vary greatly with the periodicity of forcing (−37‰ to −18‰) but are consistent with results from the Box model of the Isotopic Carbon cYCLE (BICYCLE) (*SI Appendix*, Table S1). Changes in air–sea gas exchange could therefore contribute to rapid $\delta^{13}C$-CO_2 variability.

Identifying and Diagnosing Deglacial $\delta^{13}C$-CO_2 Variability

All of the above processes can work in combination, leading to a system that is fundamentally underconstrained by the CO_2-to-$\delta^{13}C$-CO_2 relationship. Nonetheless, the changing relationship between CO_2 and $\delta^{13}C$-CO_2 with time can be combined with the model constraints to divide the data into time intervals based on the dominant processes (Fig. 3*B*). We identify four major patterns of variability of the carbon cycle spanning the length of our record: (*i*) a millennial-scale increase in CO_2 and decrease in $\delta^{13}C$-CO_2 during the early part of Heinrich Stadial 1 (17.6–15.5 ka); (*ii*) rising CO_2 with generally increasing $\delta^{13}C$-CO_2 during the later portion of Heinrich Stadial 1 (15.5–14.6 ka) and later portion of the YD (12.8–11.5 ka); (*iii*) rising CO_2 with centennial-scale negative isotopic excursions at 16.3 and 12.8 ka; and (*iv*) centennial-scale CO_2 rises with minor changes in $\delta^{13}C$-CO_2 at 14.6 and 11.5 ka. *SI Appendix*, Table S2 provides the Keeling plot intercepts for some of these intervals and Fig. 3 *C* and *D* show the divisions graphically.

From 17.6 to 15.5 ka $\delta^{13}C$-CO_2 decreases by about 0.3‰ and CO_2 increases by about 35 ppm. This distinct phase of the deglacial CO_2 rise was previously identified with less precise data and attributed to an increase in SO upwelling (11). Excluding the excursion around 16.3 ka (see below) the strong relationship between CO_2 and $\delta^{13}C$-CO_2 across this interval (R^2 = 0.97, y_0 = −8.6‰; Fig. 3*C*) is consistent with the bulk of the CO_2 increase being driven by a weakening of the efficiency of the biological pump. The decrease in atmospheric $\delta^{13}C$-CO_2 is thus consistent with either increased ocean ventilation (11, 26, 27), an increase in the ocean preformed nutrient content driven by a decrease of North Atlantic Deep Water (NADW) formation (28), or a decrease in the export of organic carbon to the deep ocean (29).

The timing of the $\delta^{13}C$-CO_2 decrease coincides with the deglacial decrease in the dust flux over Antarctica and may lead the inferred maximum in SO upwelling. By 16.0 ka, the non-sea-salt calcium flux at the Talos Dome ice core site (30) had decreased to near interglacial levels, whereas the SO opal flux recorded at 53.2°S, 5.1°E (31) was still increasing to values that peaked between 15.5 and 14.5 ka (Fig. 4*A*). Our data thus support the hypothesis that a decrease in iron fertilization was important during the earliest stages of the last deglaciation (32). The magnitude of the direct effect of iron fertilization is partially constrained by the data, suggesting an upper limit of 35 ppm CO_2 change from this mechanism. This is consistent with empirically derived estimates from the relationship between atmospheric CO_2 and Subantarctic productivity over multiple glacial–interglacial cycles (~40 ppm) (33) and the coupling of CO_2 and ice core proxies for dust delivery during the last glacial–interglacial cycle (≤ 40 ppm) (30). However, state-of-the-art biogeochemistry models simulate smaller glacial–interglacial changes due to iron fertilization between 8 and 15 ppm (34–36). Model and empirical estimates could be reconciled if other mechanisms for lowering the efficiency of the biological pump (e.g., ocean ventilation) are working in concert with iron fertilization during this interval and account for part of the 35 ppm increase in atmospheric CO_2. Possibly, a fast response of the carbon cycle to iron fertilization is superimposed on a slower change driven by upwelling, resulting in the two distinct rates of CO_2 rise during HS1.

From 15.5 to 11 ka, atmospheric CO_2 increases by 40 ppm and $\delta^{13}C$-CO_2 gradually increases (y_0 = −6.2‰; Fig. 3*C*) with a plateau during the BA (~14.6–13.0 ka) at values of 244 ± 2 ppm and −6.63 ± 0.04‰ for CO_2 and $\delta^{13}C$-CO_2, respectively. Broadly, the large increase in CO_2 and small overall change in $\delta^{13}C$-CO_2 is consistent with the atmospheric CO_2 increase being driven by changes in the $CaCO_3$ cycle, volcanic emissions, or concurrent changes in organic carbon cycle and ocean temperature. Most studies conclude that $CaCO_3$ feedbacks account for up to 30 ppm of glacial–interglacial CO_2 change (with an e-folding timescale of ~5,000 y; refs. 5, 6). Though certainly significant in controlling the glacial–interglacial CO_2 and $\delta^{13}C$-CO_2 differences, these effects are too slow to explain the rapid increases in atmospheric CO_2 around 14.75 ka (~10 ppm over 200 y) and 12.9–11.5 ka (~30 ppm over 1,500 y). Moreover, a CO_2 increase driven by only the $CaCO_3$ cycle or volcanic emissions would produce no variability in $\delta^{13}C$-CO_2. Instead, changes in $\delta^{13}C$-CO_2 of about 0.1‰ on the centennial timescale suggest that these changes are in part driven by a combination of rising SST and ^{13}C-depleted sources (i.e., ocean ventilation, land carbon). Allowing for relatively small contributions from $CaCO_3$ cycling and volcanic emissions, the $\delta^{13}C$-CO_2 data from 15.5 to 11.0 ka are consistent with a roughly equal mix of sources from rising ocean temperature and a weakened biological pump. The trend to more positive $\delta^{13}C$-CO_2 suggests that the temperature effect was slightly greater (60 ± 10%, assuming two end-member mixing). Note that any sources of atmospheric CO_2 from the $CaCO_3$ cycle or volcanic emissions would decrease the inferred absolute changes of these two

processes but have little effect on their relative contribution. The greater importance for temperature-driven changes in the later compared with the earlier part of the CO_2 rise is consistent with the increase in global surface temperature lagging the increase in atmospheric CO_2 (21).

A recent high-resolution record from the West Antarctic Ice Sheet (WAIS) Divide ice core demonstrated that rapid increases in CO_2 of about 12 ppm at both the onset of the BA (14.6 ka) and end of the YD (11.5 ka) occurred exactly coincident with abrupt increases in CH_4 and Northern Hemisphere (NH) temperature (13). Our data suggest that the effect of rising sea surface temperature (SST) on atmospheric CO_2 may be most pronounced during these two distinct intervals. Moreover, the WAIS Divide ice core revealed that Antarctic temperature remained stable or even continued to warm until ∼200 y after the onset of NH warming (37) (Fig. 4 *B* and *C*). A global temperature reconstruction, though uncertain on centennial timescales, records temperature increases of ∼1 and ∼0.5 °C at the onset of the BA and end of the YD, respectively (21). At the onset of the BA, our records show a 12-ppm increase in CO_2 and a 0.1‰ increase in $\delta^{13}C\text{-}CO_2$, consistent with SST dominating the atmospheric CO_2 budget. At the end of the YD, we observe very little change in $\delta^{13}C\text{-}CO_2$ during a 10-ppm rise in atmospheric CO_2, suggesting a balanced contribution from ^{13}C-depleted carbon sources and rising SST. This relationship between ocean warming and rising CO_2 suggests an important positive climate–carbon feedback that may be operating on the centennial timescale. These observations also constrain hypotheses that organic carbon sources explain the atmospheric CO_2 increases associated with NH temperature rise. Thawing NH permafrost at the onset of the BA (38) or ocean "flushing" events tied to the resumption of AMOC (39) would need to be compensated by carbon sinks that are more depleted in ^{13}C (i.e., a steeper vector in the Keeling plot that leads to a net increase in CO_2 and slight increase in $\delta^{13}C\text{-}CO_2$) or accompanied by sources that enrich the atmosphere in ^{13}C.

Two significant features in our record are the sharp century-scale minima in $\delta^{13}C\text{-}CO_2$ centered at 16.3 and 12.8 ka. These two events are associated with significant increases in atmospheric CO_2 of about 7 ppm and very rapid decreases in $\delta^{13}C\text{-}CO_2$ of nearly 0.2‰ (Fig. 3*D*). The higher resolution WAIS Divide record (13) indicates that the atmospheric CO_2 increase during the 16.3-ka event is greater in magnitude (∼12 ppm) and more rapid than our Taylor Glacier data resolves. The abrupt CO_2 increase at 16.3 ka could plausibly be interpreted as an event superimposed on a 3-kyr-long trend of rising atmospheric CO_2 from about 17.6–14.75 ka, whereas the 12.9-ka excursion appears to occur near the beginning of a relatively rapid atmospheric CO_2 increase from 12.9 to 11.5 ka. The 16.3-ka event is also associated with a small CH_4 increase that has been attributed to a rapid increase in Southern Hemisphere (SH) methane sources, perhaps associated with a southward excursion of the intertropical convergence zone (ITCZ) associated with Heinrich event 1 (14).

Our modeling experiments show that these features are consistent with a rapid release of terrestrial carbon to the atmosphere over a period of a few hundred years or less (accounting for the smoothing effect of gas trapping in the firn; *SI Appendix*, Fig. S10). These two events occurred during intervals of very weak monsoon strength in the northern tropics and some of the coldest conditions in the high-latitude NH (Fig. 4). Model experiments suggest that colder and drier conditions following collapse of the AMOC can drive decreases in land carbon stocks in the high-latitude NH (40). Although the global net balance in the model depends on the background climate and vegetation, net increases in atmospheric CO_2 occur under glacial conditions. Our data thus suggest a possible link between tropical CH_4 production and high-latitude terrestrial carbon pools driven by centennial-scale cold periods and/or drought during the deglaciation.

Alternatively, the minima in $\delta^{13}C\text{-}CO_2$ are consistent with rapid CO_2 increases driven in part by periods of enhanced air–sea gas exchange. As shown earlier, $\delta^{13}C\text{-}CO_2$ can be highly sensitive to changes in air–sea gas exchange. The precipitous drops in $\delta^{13}C\text{-}CO_2$ may reflect intervals of enhanced air–sea gas exchange that, in combination with other ^{13}C-depleted sources, drive increases in atmospheric CO_2.

Another possible scenario that can produce a Keeling plot intercept of less than the typical oceanic end member involves a combination of a weakening biological pump source that is moderated by a smaller CO_2 sink from decreasing SST. The combination of the two vectors could produce an intercept that is more negative (<–8.6‰) than the biological pump signature alone. Although this scenario is unlikely for the 16.3-ka event where we observe a significant and rapid increase in atmospheric CO_2 with no large SST decreases, the $\delta^{13}C\text{-}CO_2$ decrease at the onset of the YD is associated with a strong winter cooling in the NH, particularly in the North Atlantic. The subsequent recovery of $\delta^{13}C\text{-}CO_2$ following the minimum would likely require a source of atmospheric CO_2 from increasing SST, possibly from a delayed warming in the SH.

Conclusion

Many possible scenarios can explain the evolution of atmospheric CO_2 and $\delta^{13}C\text{-}CO_2$ during the deglaciation. Narrowing the range of scenarios is possible if the observed changes in carbon cycle can be consistently coupled to the climate history. We conclude by outlining one possible scenario that links our observations of centennial-scale features and the broader millennial-scale changes within the context of the deglacial climate transition (Fig. 4*A*). During the early part of HS1, the collapse of the AMOC (41) decreased heat transport to the North Atlantic. In response, large areas of the NH cooled and the SH warmed; possibly the ITCZ shifted southward and SH westerlies shifted southward or strengthened (42–44). We hypothesize that a shift of the westerlies off the SH continents and/or increased SH precipitation led to a precipitous decline in dust delivery over the Subantarctic ocean, driving up to 35 ppm of the CO_2 rise from about 17.6–15.5 ka. The southward migration of the ITCZ also led to drying in parts of the NH, possibly causing a reduction in organic land carbon, most notably around 16.3 ka. Alternatively, or additionally, the changing SH westerlies reached a threshold around 16.3 ka, in which wind speed over the SO increased, leading to enhanced air–sea gas exchange and possibly greater upwelling.

During the later half of HS1 (15.5–14.6 ka), dust deposition in the SO had fallen to interglacial levels and further CO_2 rise was driven mostly by warming ocean temperatures and an additional weakening of the biological pump, with a peak in SO upwelling or an extended interval of AMOC collapse as two possible mechanisms. During the YD (12.9–11.5 ka) most of the CO_2 increase was driven by similar processes to the later half of HS1. However, the initial rise in CO_2 during the YD could have been driven by either a second loss of land carbon or renewed enhancement of SH westerlies. At the onset of the BA (14.6 ka) and end of the YD (11.5 ka) significant warmings in the NH and continued warming around Antarctica likely contributed to the centennial-scale increases in atmospheric CO_2.

The $\delta^{13}C\text{-}CO_2$ record shows that the deglacial increase in atmospheric CO_2 occurred in a series of steps, each with a $\delta^{13}C$ fingerprint that suggests that different mechanisms may have been triggered at various times during the deglacial transition. Early in the transition, the decrease in $\delta^{13}C\text{-}CO_2$ is consistent with (albeit not uniquely) a combination of atmospheric CO_2 sources from respired organic carbon that exceeded sources from rising ocean temperature. This suggests that the initial trigger for the deglacial CO_2 rise involved either an ocean circulation or ocean biological process. Later in the transition, the relatively stable $\delta^{13}C\text{-}CO_2$, punctuated by centennial-scale changes, suggests a combination of sources that could include changes in the $CaCO_3$ cycle or volcanic emissions, but most likely reflects a balanced contribution of respired organic carbon and rising ocean temperature that strengthens and weakens over time. At least twice during the deglaciation a rapid release of ^{13}C-depleted carbon to the atmosphere may have occurred over a few centuries, suggesting that abrupt and significant releases of CO_2 to the atmosphere may be common nonlinear features of Earth's carbon cycle. Further work on defining the isotopic signature of glacial–interglacial CO_2 mechanisms across a

suite of carbon cycle models could yield a more precise understanding of CO_2 sources during the deglaciation.

ACKNOWLEDGMENTS. We thank Tanner Kuhl, Robb Kulin, and Paul Rose for assistance in the field and Fortunat Joos, Laurie Menviel, and Andreas Schmittner for sharing model output. We thank Mathis Hain and an anonymous reviewer for comments that improved the paper. We are grateful for technical support from NSF-funded Ice Drilling Design and Operations (University of Wisconsin) and the OSU/CEOAS Stable Isotope Laboratory, in particular Andy Ross. This work was funded by NSF Grants ANT 0838936 (Oregon State University) and ANT 0839031 (Scripps Institution of Oceanography). Further support came from the Marsden Fund Council from New Zealand Government funding, administered by the Royal Society of New Zealand and NIWA under Climate and Atmosphere Research Programme CAAC1504 (to H.S.). T.K.B. was partially supported by the Comer Science and Education Foundation.

1. Berner W, Oeschger H, Stauffer B (1980) Information on the CO_2 cycle from ice core Studies. *Radiocarbon* 22(2):227–235.
2. Delmas RJ, Ascencio J-M, Legrand M (1980) Polar ice evidence that atmospheric CO_2 20,000 yr BP was 50% of present. *Nature* 284(5752):155–157.
3. Kohfeld KE, Ridgwell A (2009) Glacial-interglacial variability in atmospheric CO_2. *Geophys Monogr Ser* 187:251–286.
4. Ciais P, et al. (2013) Carbon and other biogeochemical cycles. *Climate Change: The Physical Science Basis.* Contribution of Working Group I to the Fifth Assessment Report of the Intergovernmental Panel on Climate Change eds Stocker, T.F., et al. (Cambridge Univ Press, Cambridge, UK), pp 465–570.
5. Toggweiler JR (1999) Variation of atmospheric CO_2 by ventilation of the ocean's deepest water. *Paleoceanography* 14(5):571–588.
6. Hain MP, Sigman DM, Haug GH (2010) Carbon dioxide effects of Antarctic stratification, North Atlantic Intermediate Water formation, and subantarctic nutrient drawdown during the last ice age: Diagnosis and synthesis in a geochemical box model. *Global Biogeochem Cycles* 24:GB4023.
7. Köhler P, Fischer H, Schmitt J, Munhoven G (2006) On the application and interpretation of Keeling plots in paleo climate research - Deciphering $\delta^{13}C$ of atmospheric CO_2 measured in ice cores. *Biogeosciences* 3(4):539–556.
8. Köhler P, Fischer H, Schmitt J (2010) Atmospheric $\delta^{13}CO_2$ and its relation to pCO_2 and deep ocean $\delta^{13}C$ during the late Pleistocene. *Paleoceanography* 25(1), 10.1029/2008pa001703.
9. Smith HJ, Fischer H, Wahlen M, Mastroianni D, Deck B (1999) Dual modes of the carbon cycle since the Last Glacial Maximum. *Nature* 400(6741):248–250.
10. Lourantou A, et al. (2010) Constraint of the CO_2 rise by new atmospheric carbon isotopic measurements during the last deglaciation. *Global Biogeochem Cycles* 24: GB2015.
11. Schmitt J, et al. (2012) Carbon isotope constraints on the deglacial CO_2 rise from ice cores. *Science* 336(6082):711–714.
12. Bauska TK, Brook EJ, Mix AC, Ross A (2014) High-precision dual-inlet IRMS measurements of the stable isotopes of CO_2 and the N_2O/CO_2 ratio from polar ice core samples. *Atmos Meas Tech* 7:3825–3837.
13. Marcott SA, et al. (2014) Centennial-scale changes in the global carbon cycle during the last deglaciation. *Nature* 514(7524):616–619.
14. Rhodes RH, et al. (2015) Enhanced tropical methane production in response to iceberg discharge in the North Atlantic. *Science* 348(6238):1016–1019.
15. Keeling CD (1958) The concentration and isotopic abundances of atmospheric carbon dioxide in rural areas. *Geochim Cosmochim Acta* 13(4):322–334.
16. Fischer H, et al. (2007) Reconstruction of millennial changes in dust emission, transport and regional sea ice coverage using the deep EPICA ice cores from the Atlantic and Indian Ocean sector of Antarctica. *Earth Planet Sci Lett* 260(1-2): 340–354.
17. Menviel L, Joos F, Ritz SP (2012) Simulating atmospheric CO_2, ^{13}C and the marine carbon cycle during the Last Glacial–Interglacial cycle: Possible role for a deepening of the mean remineralization depth and an increase in the oceanic nutrient inventory. *Quat Sci Rev* 56:46–68.
18. Tschumi T, Joos F, Gehlen M, Heinze C (2011) Deep ocean ventilation, carbon isotopes, marine sedimentation and the deglacial CO_2 rise. *Clim Past* 7(3): 771–800.
19. Schmittner A, Lund DC (2015) Early deglacial Atlantic overturning decline and its role in atmospheric CO_2 rise inferred from carbon isotopes ($\delta^{13}C$). *Clim Past* 11(2):135–152.
20. Yu J, et al. (2010) Loss of carbon from the deep sea since the Last Glacial Maximum. *Science* 330(6007):1084–1087.
21. Shakun JD, et al. (2012) Global warming preceded by increasing carbon dioxide concentrations during the last deglaciation. *Nature* 484(7392):49–54.
22. Broecker WS, Peng T-H (1987) The role of $CaCO_3$ compensation in the glacial to interglacial atmospheric CO_2 change. *Global Biogeochem Cycles* 1(1):15–29.
23. Boyle EA (1988) The role of vertical chemical fractionation in controlling late Quaternary atmospheric carbon dioxide. *J Geophys Res* 93(C12):15701–15714.
24. Schneider R, Schmitt J, Köhler P, Joos F, Fischer H (2013) A reconstruction of atmospheric carbon dioxide and its stable carbon isotopic composition from the penultimate glacial maximum to the last glacial inception. *Clim Past* 9(6): 2507–2523.
25. Stephens BB, Keeling RF (2000) The influence of Antarctic sea ice on glacial-interglacial CO_2 variations. *Nature* 404(6774):171–174.
26. Toggweiler JR, Russell JL, Carson SR (2006) Midlatitude westerlies, atmospheric CO_2, and climate change during the ice ages. *Paleoceanography* 21:PA2005.
27. Skinner LC, Fallon S, Waelbroeck C, Michel E, Barker S (2010) Ventilation of the deep Southern Ocean and deglacial CO_2 rise. *Science* 328(5982):1147–1151.
28. Schmittner A, Galbraith ED (2008) Glacial greenhouse-gas fluctuations controlled by ocean circulation changes. *Nature* 456(7220):373–376.
29. Martin JH (1990) Glacial-interglacial CO_2 change: The Iron Hypothesis. *Paleoceanography* 5(1):1–13.
30. Schüpbach S, et al. (2013) High-resolution mineral dust and sea ice proxy records from the Talos Dome ice core. *Clim Past* 9(6):2789–2807.
31. Anderson RF, et al. (2009) Wind-driven upwelling in the Southern Ocean and the deglacial rise in atmospheric CO_2. *Science* 323(5920):1443–1448.
32. Broecker WS, McGee D (2013) The ^{13}C record for atmospheric CO_2: What is it trying to tell us? *Earth Planet Sci Lett* 368(0):175–182.
33. Jaccard SL, et al. (2013) Two modes of change in Southern Ocean productivity over the past million years. *Science* 339(6126):1419–1423.
34. Archer D, Winguth A, Lea D, Mahowald N (2000) What caused the glacial/interglacial atmospheric pCO_2 cycles? *Rev Geophys* 38(2):159–189.
35. Bopp L, Kohfeld KE, Le Quéré C, Aumont O (2003) Dust impact on marine biota and atmospheric CO_2 during glacial periods. *Paleoceanography* 18(2):1046.
36. Parekh P, Dutkiewicz S, Follows M, Ito T (2006) Atmospheric carbon dioxide in a less dusty world. *Geophys Res Lett* 33(3) doi: 10.1029/2005GL025098.
37. WAIS Divide Project Members (2015) Precise interpolar phasing of abrupt climate change during the last ice age. *Nature* 520(7549):661–665.
38. Köhler P, Knorr G, Bard E (2014) Permafrost thawing as a possible source of abrupt carbon release at the onset of the Bølling/Allerød. *Nat Commun* 5:5520.
39. Chen T, et al. (2015) Synchronous centennial abrupt events in the ocean and atmosphere during the last deglaciation. *Science* 349(6255):1537–1541.
40. Köhler P, Joos F, Gerber S, Knutti R (2005) Simulated changes in vegetation distribution, land carbon storage, and atmospheric CO_2 in response to a collapse of the North Atlantic thermohaline circulation. *Clim Dyn* 25(7-8):689–708.
41. McManus JF, Francois R, Gherardi JM, Keigwin LD, Brown-Leger S (2004) Collapse and rapid resumption of Atlantic meridional circulation linked to deglacial climate changes. *Nature* 428(6985):834–837.
42. Wang X, et al. (2004) Wet periods in northeastern Brazil over the past 210 kyr linked to distant climate anomalies. *Nature* 432(7018):740–743.
43. Cheng H, et al. (2009) Ice age terminations. *Science* 326(5950):248–252.
44. Denton GH, et al. (2010) The last glacial termination. *Science* 328(5986):1652–1656.
45. Elsig J, et al. (2009) Stable isotope constraints on Holocene carbon cycle changes from an Antarctic ice core. *Nature* 461(7263):507–510.
46. Andersen KK, et al.; North Greenland Ice Core Project members (2004) High-resolution record of Northern Hemisphere climate extending into the last interglacial period. *Nature* 431(7005):147–151.
47. WAIS Divide Project Members (2013) Onset of deglacial warming in West Antarctica driven by local orbital forcing. *Nature* 500(7463):440–444.
48. Wu J, Wang Y, Cheng H, Edwards LR (2009) An exceptionally strengthened East Asian summer monsoon event between 19.9 and 17.1 ka BP recorded in a Hulu stalagmite. *Sci China Ser. Earth Sci* 52(3):360–368.